J|A|C|S
COMMUNICATIONS

Published on Web 11/15/2006

Structure of the Oxidized Active Site of Galactose Oxidase from Realistic In Silico Models

Dalia Rokhsana, David M. Dooley,* and Robert K. Szilagyi*

Department of Chemistry and Biochemistry, Montana State University, Bozeman, Montana 59717

Received April 18, 2006; E-mail: dmdooley@montana.edu; szilagyi@montana.edu

Galactose oxidase (GO) is a post-translationally modified enzyme produced by the fungus *Dactylium dendroides*.[1] The active site consists of two one-electron redox units, a Cu(II) ion, and a crosslinked Y272•-C228 radical cofactor, which together are responsible for the catalytic activity. GO catalyzes the two-electron oxidation of a broad range of primary alcohols to the corresponding aldehydes, with the concomitant reduction of dioxygen to hydrogen peroxide.[1] GO displays three distinct oxidation states: oxidized [Cu(II)-Y•, green], semireduced [Cu(II)-Y, blue], and fully reduced [Cu(I)-Y, colorless].[2] It has been assumed that the oxidized and fully reduced states participate in the catalytic cycle, but the semireduced state may also be physiologically relevant. Hence, structural knowledge of these distinct redox states are essential to understand the molecular mechanism of GO.

The crystal structure of the [Cu(II)-Y] state at pH 7 (1.9 Å resolution) revealed a square pyramidal Cu(II) geometry (Figure 1).[3,4] Spectroscopic studies provided further insights into the copper coordination environment.[5,6] EXAFS studies[6] suggested that the coordination environment of [Cu(II)-Y•] GO is similar to that of the [Cu(II)-Y] state with average bond distances of Cu−N = 1.95 and Cu−O = 1.96 Å. These distances are considerably shorter than what has been observed in the crystal structure (Figure 1). Magnetic susceptibility measurements of [Cu(II)-Y•] were consistent with antiferromagnetic coupling ($J > 200$ cm^{-1}) between the protein radical and the Cu(II) ion, resulting in a singlet ground state.[5] In addition, spectroscopic studies have demonstrated that the protein radical is located on the Y272−C228 cofactor.[7−10]

Recently, computational studies employing small active site models on the catalytic cycle of GO have been reported.[11,12] The results provided a useful context for understanding the mechanistic data.[5] Interestingly, it was suggested that the protein radical is located on the axial Y495 rather than the equatorial Tyr-Cys crosslinked cofactor prior to proton transfer, but no further structural details of the active site were reported.[11]

We have employed a systematic in silico approach to investigate the coordination geometry and electronic structure of the [Cu(II)-Y•] state of GO, using spectroscopically calibrated hybrid density-functional theory (DFT).[13] We report here intriguing results for the [Cu(II)-Y•] state of GO, which provides new perspectives on the active-site structure and catalytic mechanism of GO.

In order to develop an accurate and reliable active-site model for the oxidized GO, we generated multiple models starting from the semireduced GO crystal structure (Figure 1) and evaluated these models by comparing the calculated electronic and magnetic properties with key experimental data (electronic absorption spectra and J values, respectively). We have assessed computational models spanning a truncated model (H496 and H581 = imidazole, Y495 = phenol, Y272 = thiophenol, and H_2O) to an extended model system with 148 atoms. The extended model included the α-carbon of each residue coordinated to the Cu(II), the protein backbone between Y495 and H496, an additional H_2O within hydrogen-bonding distance from both Tyr residues (~3 Å in the crystal structure), distal residues Y405 (protonated), R330, W290 (π-stacked with Y272−C228 cofactor), and an additional water to model the water exposed active-site residue, Y495. Optimization of the model was performed using the redundant coordinate system and Berny optimization algorithm. The convergence criteria were set to 0.002 Å/au and 0.006 au rms change in gradient and displacement, respectively. All calculations were carried out by employing the B(38HF)P86 functional with triple-ζ (VTZ*) and double-ζ with polarization (6-31G(d)) basis sets for Cu and all other atoms, respectively. In addition to fixing the α-carbons of all residues, the conformation of the guanidium group of R330 was also constrained by fixing δN, ϵC, χN to avoid unreasonable conformation changes that were inconsistent with the structural data.

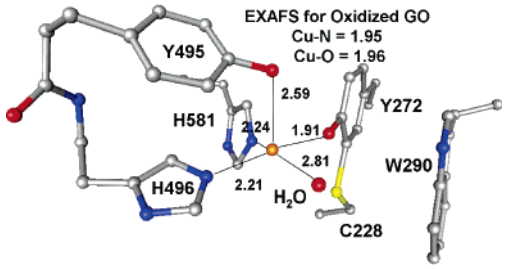

Figure 1. Crystal structure of the active site of GO in the semireduced [Cu(II)-Y] state at 1.9 Å resolution with selected Cu−ligand distances (PDB ID 1GOG).[3]

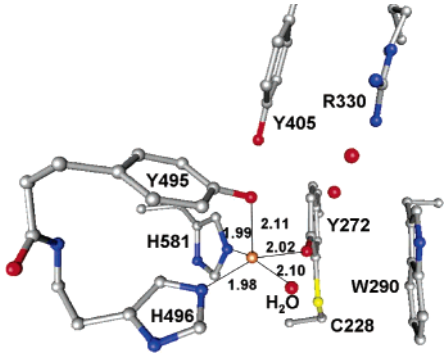

Figure 2. Optimized structure of the oxidized [Cu(II)-Y•] GO model.

The optimized structure reveals a stable five-coordinate pyramidal coordination geometry with Y495 in an axial position and four other ligands in equatorial positions with cis and trans ligand−Cu−ligand bond angles of 77−94°, 155°, and 159°, respectively (Figure 2). As suggested (see above), the overall coordination geometry of the copper site in [Cu(II)-Y•] is quite similar to [Cu(II)-Y] with considerable deviations in the Cu−ligand bond distances. The average Cu−N and Cu−O distances (1.99 and 2.06 Å) are in reasonable agreement with the EXAFS data.

Furthermore, the calculated electronic structure of the oxidized [Cu(II)-Y•] state suggests a normal bonding description involving

10.1021/ja062702f CCC: $33.50

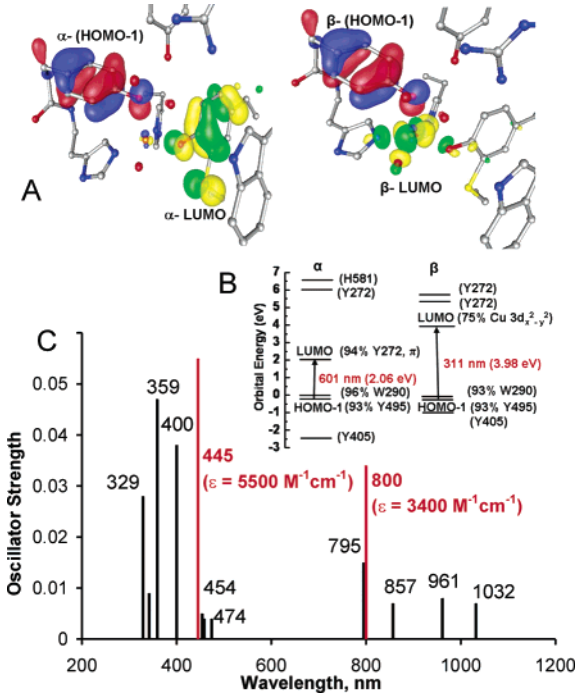

Figure 3. (A) Molecular orbitals (isosurface value = ±0.05) showing HOMO-1 and LUMO of both α- and β-manifolds from Kohn−Sham orbital analysis; (B) Kohn−Sham orbital and their relative orbital energies in electron volts; (C) oscillator strength vs wavelength from TDDFT analysis (calcd, black; exptl, red) of the [Cu(II)-Y•] GO model.

a $3d_{x^2-y^2}$ orbital with 0.76 e$^-$ spin density located on the Cu(II) ion, and the remaining 0.24 e$^-$ is delocalized onto the σ-bonded equatorial ligands. The Y272•-C228 radical has ∼0.91 e$^-$ spin density in an out-of-plane π_4 orbital (for labeling see supporting material Figure S1) with the opposite sign to the spin on Cu(II). This contains ∼0.24 e$^-$ spin delocalization onto the sulfur atom of C228, which parallels the conclusion drawn from studies on synthetic active site GO models.[9,14] The $\pi-\pi$ stacking between W290 and Y272•-C228 and constraints from αC-atoms of Y272, C228, and W290 maintain a cofactor orientation (Cu−O−C bond angle α = 125° and dihedral angle between equatorial plane of Cu coordinated ligands and tyrosyl ring plane β = ∼82°) that results in a diamagnetic ground state.[15] A Kohn−Sham molecular orbital energy diagram for the oxidized model is shown in Figure 3. The electronic transitions between HOMO-1 and LUMO orbitals at 311 and 601 nm in the spin-down (β) and spin-up (α) manifold, respectively, can be assigned as ligand-to-metal charge transfer (LMCT) and ligand-to-ligand charge transfer (LLCT) excitations. The former corresponds to the tyrosinate (Y495) to $3d_{x^2-y^2}$ orbital of Cu(II), $\pi_4 \rightarrow \sigma^*$, and the latter to tyrosinate (Y495) to tyrosyl (Y272) radical, $\pi_4 \rightarrow \pi_4$ (Figure 3A). Time-dependent DFT (TDDFT) analysis provides an improved fit between the experimental and calculated band positions and intensities (Figure 3C). Significant oscillator strengths were obtained for transitions at 795 nm (radical Y272 $\pi_3 \rightarrow \pi_4$), 400 nm (radical Y272 $\pi_2 \rightarrow \pi_4$), and 359 nm (H496 (π) and Y272 (π_4) to σ^* of Cu(II) $3d_{x^2-y^2}$). These are in general consistent with resonance Raman (rR) assignments except that the TDDFT calculations do not predict substantial contributions from Y495.[16,17] Only the extended computational model containing all residues that have been shown to affect the active-site structure reproduces the absorption spectra (experimental: 445 and 800 nm; calculated from TDDFT, 400 and 795 nm) (Figure 3C) and the antiferromagnetic coupling J (∼752 cm^{-1}). Other functionals, such as B3LYP and BP86, provide poor agreement for the excitation energies than the spectroscopically calibrated B(38HF)P86 that we employed. Furthermore, we have completed the optimization of a larger model with 214 atoms containing additional second and third coordination-shell residues (Gln406, His334, Tyr329, Thr580, and Gly513), which is fully consistent with the Cu coordination environment of the extended model described in this paper.

It has already been shown experimentally[4,18] that residues of the second coordination shell influence the substrate binding and catalysis in GO. Our current computational study also emphasizes the importance of second coordination-sphere residues and provides tools to dissect their contributions to the active-site structure and catalytic activity. Inclusion of outersphere ligands in the in silico models was crucial to obtain the spectroscopically correct electronic structure for the active site. The hydrogen-bonding interactions involving the O atom of Y495 play a critical role in modulating the spin density distribution and the singlet−triplet energy gap. In addition, the $\pi-\pi$ stacking of W290 and Tyr•-Cys cofactor also affects the spin density distribution of the cofactor radical. Y495 and W290 are both exposed to water and thus inclusion of explicit solvent water molecules hydrogen bonding to these residues are also essential. The structural information from our computational studies provides a strong foundation for further investigating the redox-dependent changes in the GO active site and the molecular mechanism.

Acknowledgment. We gratefully acknowledge the support of this research by NIH Grant (D.R. and D.M.D.) GM 27659 and by NSF EPSCoR and ONR CBIN (R.K.S.)

Supporting Information Available: Optimized coordinates, orbital energy levels for tyrosine, detailed MO and TDDFT analyses. This material is available free of charge via the Internet at http://pubs.acs.org.

References

(1) Avigad, G.; Amaral, D.; Asensio, C.; Horecker, B. L. *J. Biol. Chem.* **1962**, *237*, 2736.
(2) Whittaker, M. M.; Whittaker, J. W. *J. Biol. Chem.* **1988**, *263*, 6074.
(3) Ito, N.; Phillips, S. E. V.; Stevens, C.; Ogel, Z. B.; McPherson, M. J.; Keen, J. N.; Yadav, K. D. S.; Knowles, P. F. *Nature* **1991**, *350*, 87.
(4) Ito, N.; Phillips, S. E. V.; Yadav, K. D. S.; Knowles, P. F. *J. Mol. Biol* **1994**, *238*, 794.
(5) Whittaker, J. W. *Chem. Rev.* **2003**, *103*, 2347.
(6) Knowles, P. F.; Brown, R. D.; Koenig, S. H.; Wang, S.; Scott, R. A.; McGuirl, M. A.; Brown, D. E.; Dooley, D. M. *Inorg. Chem.* **1995**, *34*, 3895.
(7) Babcock, G. T.; El-Deeb, M. K.; Sandusky, P. O.; Whittaker, M. M.; Whittaker, J. W. *J. Am. Chem. Soc.* **1992**, *114*, 3727.
(8) McGlashin, M. L.; Eads, D. D.; Spiro, T. G.; Whittaker, J. W. *J. Phys. Chem.* **1995**, *99*, 4918.
(9) Gerfen, G. J.; Bellew, B. F.; Griffin, R. G.; Singel, D. J.; Ekberg, C. A.; Whittaker, J. W. *J. Phys. Chem.* **1996**, *100*, 16739.
(10) Whittaker, M. M.; Chuang, Y. Y.; Whittaker, J. W. *J. Am. Chem. Soc.* **1993**, *115*, 10029.
(11) Himo, F.; Eriksson, L. A.; Maseras, F.; Siegbahn, P. E. M. *J. Am. Chem. Soc.* **2000**, *122*, 8031.
(12) Rothlisberger, U.; Carloni, P.; Doclo, K.; Parrinello, M. *J. Biol. Inorg. Chem.* **2000**, *5*, 236.
(13) Szilagyi, R. K.; Solomon, E. I. *Curr. Opin. Chem. Biol.* **2002**, *6*, 250.
(14) Itoh, S.; Taki, M.; Kumei, H.; Takayama, S.; Nagatomo, S.; Kitagawa, T.; Sakurada, N.; Arakawa, R.; Fukuzumi, S. *Inorg. Chem.* **2000**, *39*, 3708.
(15) Muller, J.; Weyhermuller, T.; Bill, E.; Hildebrandt, P.; Ould-Moussa, L.; Glaser, T.; Wieghardt, K. *Angew. Chem., Int. Ed.* **1998**, *37*, 616.
(16) McGlashen, M. L.; Eads, D. D.; Spiro, T. G.; Whittaker, J. W. *J. Phys. Chem.* **1995**, *99*, 4918.
(17) Whittaker, M. M.; DeVito, V. L.; Asher, S. A.; Whittaker, J. W. *J. Biol. Chem.* **1989**, *264*, 7104.
(18) Rogers, M. S.; Knowles, P. F.; Baron, A. J.; McPherson, M. J.; Dooley, D. M. *Inorg. Chim. Acta* **1998**, *275*−276, 175.

JA062702F